LOOKING FOR $O(N)$ NAVIER-STOKES SOLUTIONS ON NON-STRUCTURED MESHES [1]

Eric MORANO [2]
ICASE, NASA Langley Research Center
Hampton, VA, USA

Alain DERVIEUX
INRIA
BP 93, 06902 Sophia Antipolis Cedex, France

SUMMARY

Multigrid methods are good candidates for the resolution of the system arising in Numerical Fluid Dynamics. However, the question is to know if those algorithms which are efficient for the Poisson equation on structured meshes will still apply well to the Euler and Navier-Stokes equations on unstructured meshes. The study of elliptic problems leads us to define the conditions where a Full Multigrid strategy has $O(N)$ complexity. The aim of this paper is to build a comparison between the elliptic theory and practical CFD problems.

First, as an introduction, we will recall some basic definitions and theorems applied to a model problem. The goal of this section is to point out the different properties that we need to produce an FMG algorithm with $O(N)$ complexity. Then, we will show how we can apply this theory to the fluid dynamics equations such as Euler and Navier-Stokes equations. At last, we present some results which are 2nd-order accurate and some explanations about the behaviour of the FMG process.

INTRODUCTION

One first important element is the mesh independent convergence speed. Hackbush, in [1] for example, proposes a demonstration of this property. It is done in the special case of an elliptic problem on structured nested meshes. We want to evaluate the properties that we must keep in order to get the mesh independent convergence speed when we use unstructured non-embedded meshes.

The problem to be solved is the following:

$$\begin{cases} \Delta u = f \text{ on } \Omega \text{ convex polygonal domain} \\ u\,|_{\partial\Omega} = 0 \end{cases} \tag{1}$$

$$u \in H_1^0(\Omega) \text{ and } f \in L^2(\Omega)$$

The discretization is a usual linear P1-Galerkin finite element. Thus, we get a discrete space $\mathcal{H}_h$ whose dimension is equal to N_h (number of nodes), and where the subscript h indicates the mesh

[1]Work partly supported by DRET Groupe 6 under contract.
[2]Supported by INRIA and "Région Provence-Alpes-Côte d'Azur" (France), and ICASE (USA).

size. The resulting problem consists now in solving the linear system:

$$A_h\, u_h \;=\; f_h \tag{2}$$

We may evaluate the discretization error thanks to the Aubin-Nitsche's theorem and usual regularity:

$$\|u - u_h\|_{L^2} \;\leq\; C_2\, h^2\, \|u\|_{H^2} \;\leq\; C_3\, h^2\, \|f\|_{L^2} \tag{3}$$

The linear system (2) may incur a lot of CPU time because of its size (large number of nodes). The idea is then to use a second finite element subspace $\mathcal{H}_H$ whose dimension N_H is less than the previous one (usually $H = 2h$). We have then the following relationship between both spaces (also called grids):

$$\begin{array}{ccc} & \overset{A_H^{-1}}{\longrightarrow} & \\ \mathbb{R}^{N_H} & & \mathbb{R}^{N_H} \\ R \;\uparrow & & \downarrow \;P \\ \mathbb{R}^{N_h} & & \mathbb{R}^{N_h} \\ & \underset{A_h^{-1}}{\longrightarrow} & \end{array}$$

where P and R are linear interpolations (transfer operators). The iterative process can be written as:

$$u_h^{n+1} \;=\; M_h\, u_h^n + N_h\, f_h \;\text{ where: }\; M_h \;=\; S_h^{\nu_2}\, (I - P\, A_H^{-1}\, R\, A_h)\, S_h^{\nu},\; S_h = I - \omega D_h^{-1} A_h$$

(S defines the basic iterative smoother, ν_1 and ν_2 the number of pre- and post-relaxations). Such a process converges if $\|M_h\| \;<\; 1$. A very important property of this kind of method is that the convergence is independent of the mesh size. In order to simplify the notations (and the study) we rewrite M_h as the following ideal-2-grid operator [2]:

$$M_h \;=\; (A_h^{-1} - P\, A_H^{-1}\, R)(A_h\, S_h^{\nu}) \tag{4}$$

The norms of both factors of the right hand side of the equation (4) will determine the norm of M_h:

- The smoothing property:

$$\begin{array}{rcl} \|A_h\, S_h^{\nu}\| & \leq & 1/h^2\, \eta(\nu) \\ \lim\limits_{\nu\to\infty} \eta(\nu) & = & 0 \end{array} \tag{5}$$

  depends a lot on the basic smoothing process, and, we will not give any details.

- The approximation property is:

$$\|A_h^{-1} - P\, A_H^{-1}\, R\,\| \;=\; O(h^2) \tag{6}$$

  Let us focus on (6): it takes into account the transfer operators, and overall, represents the difference that exists between the solution on the fine grid and the solution on the coarse grid.

An MG scheme that exhibits these properties will result in a convergence speed that is independent of the mesh size:

$$\forall \rho\; \exists \nu(\rho) \text{ such that } \|M_h\, v_h - u_h\| \leq \rho \|v_h - u_h\|$$

We may notice that demonstrating the approximation property leads to the evaluation of the following quantity:

$$\|p_h P A_H^{-1} R r_h - A^{-1}\|$$

For nested meshes, thanks to (3), one can easily derive this from the following equality:

$$p_h P = p_H$$

On the other hand, for unnested meshes, $p_h P$ is not equal to p_H and this evaluation is more difficult. Actually, it is the same as evaluating the difference between two interpolated solutions. Zhang [3], thanks to Bank-Dupont's theory, proposes such an evaluation.

Remark: The multigrid iterative V-cycle algorithm can easily be deduced from the previous 2-grid algorithm recursively. It maintains the convergence speed independently of the mesh size and has an $O(N \log N)$ complexity.

In order to apply the previous result of convergence, we propose to use a Full Multigrid (FMG) strategy (proposed by Brandt in [4]). A well known result is the one given by Hackbush in [1], which is given below:

Theorem: We note: κ the consistency order, $C_2 = \max_{1 \leq k \leq l} (h_{k-1}/h_k)^\kappa$ the ratio of accuracy between two solutions, S the reduction factor of the MG process, i the number of MG iterations applied to reach the solution $\tilde{u}_k^i$. If u_k is the solution of the discrete problem, we have:

$$\|\tilde{u}_k^i - u_k\| \leq C_3^i C_1 h_k^\kappa \quad \text{with} \quad C_3^i = \frac{S^i}{1 - C_2 S^i}.$$

Assuming that $C_2 = 2^\kappa$, we deduce the exact number of cycles in each FMG phase to solve the 1st-order problem ($S^i \leq 1/4$) and the 2nd-order problem ($S^i \leq 1/8$). The number of cycles i in each phase is constant, which leads to an algorithm that has $O(N)$ complexity.

Once again, the relative interpolation error [1] conditions the quality of the initialization in each phase. Thus, in order to stay close to the ideal scheme (where the different subspaces are nested), we propose to build meshes where:

- The mesh size ratio is close to 2,
- The triangles aspect ratio is locally comparable in the whole domain.

We have thus identified the different necessary ingredients to build an algorithm having $O(N)$ complexity:

1. A sequence of grids,
2. A basic smoother (ex: Jacobi,Gauss-Seidel),
3. Intergrid transfer operators (ex: linear interpolations),
4. MG algorithm (ex: V-cycle, W-cycle),
5. FMG strategy.

We may now apply it to more complex fluid dynamics problems such as the resolution of the Navier-Stokes/Euler equations.

We recall first the formulation of the steady Navier-Stokes equations:

$$\frac{\partial F(W)}{\partial x}+\frac{\partial G(W)}{\partial y}=\frac{1}{Re}\left(\frac{\partial R(W)}{\partial x}+\frac{\partial S(W)}{\partial y}\right)\ ,\quad W=(\rho,\rho u,\rho v,E)^T\ ,$$

$$F(W)=\begin{pmatrix}\rho u\\ \rho u^2+p\\ \rho uv\\ (E+p)u\end{pmatrix}\ G(W)=\begin{pmatrix}\rho v\\ \rho uv\\ \rho v^2+p\\ (E+p)v\end{pmatrix}\ ,\quad \mathbb{F}(W)=\begin{pmatrix}F(W)\\ G(W)\end{pmatrix}\ , \tag{7}$$

$$R(W)=\begin{pmatrix}0\\ \tau_{xx}\\ \tau_{xy}\\ u\tau_{xx}+v\tau_{xy}+\dfrac{\gamma\kappa}{Pr}\dfrac{\partial e}{\partial x}\end{pmatrix}S(W)=\begin{pmatrix}0\\ \tau_{xy}\\ \tau_{yy}\\ u\tau_{xy}+v\tau_{yy}+\dfrac{\gamma\kappa}{Pr}\dfrac{\partial e}{\partial y}\end{pmatrix}\ ,$$

$$p=(\gamma-1)\left(E-\tfrac{1}{2}\,\rho\,(u^2+v^2)\right)\ ,\quad e=C_vT=\tfrac{E}{\rho}-\tfrac{1}{2}(u^2+v^2)\ ,$$

where $\gamma=1.4$ is the ratio of specific heats, T is the temperature, μ and κ are the normalized viscosity and thermal conductivity coefficients. The components of the Cauchy stress tensor τ_{xx}, τ_{xy} and τ_{yy} are given by:

$$\tau_{xx}=\frac{2}{3}\mu\left(2\frac{\partial u}{\partial x}-\frac{\partial v}{\partial y}\right)\ ,\ \tau_{yy}=\frac{2}{3}\mu\left(2\frac{\partial v}{\partial y}-\frac{\partial u}{\partial x}\right)\ ,\ \tau_{xy}=\mu\left(\frac{\partial u}{\partial y}+\frac{\partial v}{\partial x}\right)$$

$Re=\rho_0U_0L_0/\mu_0$ is the Reynolds number and $Pr=\mu_0C_p/\kappa_0$ is the Prandtl number, where ρ_0, U_0, L_0 and μ_0 denote respectively the characteristic density, velocity, length and diffusivity of the considered flow. It is easily seen that, if the right-hand side is equal to zero, then we recover the Euler equations. The inlet conditions are defined by the farfield flow. For Euler flows, we impose the slip condition on the wall ($\vec{V}.\vec{n}\ =\ 0$), and for Navier-Stokes flows, on the wall, the no-slip condition ($\vec{V}=\vec{0}$) and the isothermal condition ($T=T_b$). The discretization is given by a mixed FEM/FVM formulation [5], where the mesh is a finite-element type (triangles), on which we construct control-cells (FVM) in order to solve the variational formulation of the equations, such as, for the Euler flows:

$$\sum_{j\in K(i)}\left[\int_{\partial C_j}\vec{v}_i.\vec{\mathbb{F}}(W)d\sigma\right]+\int_{\mathrm{Im}\partial C_i}\vec{v}_i.\vec{\mathbb{F}}(W)d\sigma=\frac{1}{Re}\left[\sum_{\triangle,i\in\triangle}\iint_{\triangle}\left(R\frac{\partial\Psi_i^{\triangle}}{\partial x}+S\frac{\partial\Psi_i^{\triangle}}{\partial y}\right)dxdy\right] \tag{8}$$

The computation of the fluxes, appearing in (8), between two cells, is managed by Roe's numerical flux vector splitting in the domain, and by the Steger-Warming numerical flux vector splitting for the farfield boundaries. The 2nd-order accurate scheme is obtained by the use of the MUSCL method developed by van Leer [6]. We solve the discrete equations with non-linear relaxation algorithms [6],

namely here the multistage Jacobi algorithm [2, 7]:

$$\left[\begin{array}{c} W_j^{(0)} = W_j^{\alpha} \\ \text{For } ks = 1 \text{ to } nstage \\ [D]_{i,j} = \left[\dfrac{\partial \Phi}{\partial W_j}(W_i^{\alpha}, W_j^{(ks)}; \vec{\eta}_{i,j})\right] \\ W_j^{(ks+1)} = W_j^{(0)} - \omega \ C_{ks} \sum\limits_{i \in K(j)} [D]_{i,j}^{-1} \ \Phi(W_i^{\alpha}, W_j^{(ks)}; \vec{\eta}_{i,j}) \\ W_j^{\alpha+1} = W_j^{(nstage)} \end{array}\right. \tag{9}$$

Let us now look at the meshes. We start with an initial given fine mesh Fig.1.a. Finer meshes are

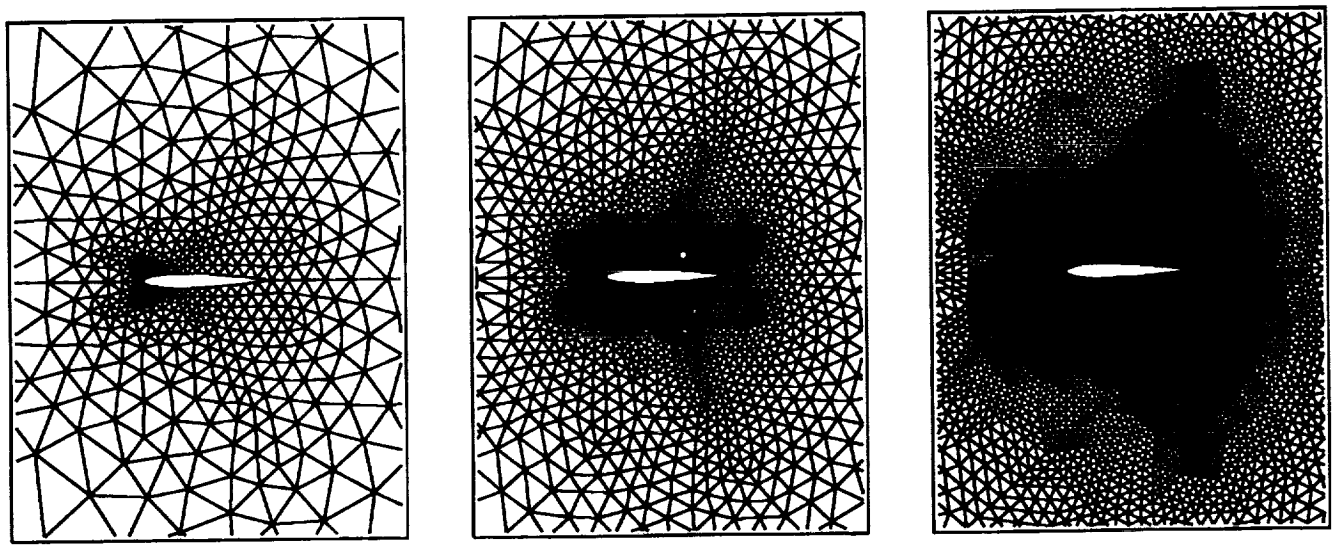

a. Initial 800 nodes b. 3114 nodes c. Finest 12284 nodes

Figure 1: NACA0012 fine meshes.

obtained by triangle subdivision (Fig.1.b,.c). Then, we use a coarsening algorithm due to Guillard [8] to build coarser meshes, from the initial one. This produces a sequence of node-embedded meshes (Fig.2.a,.b,.c). We get 6 meshes for the NACA0012 profile, where the finest has 12284 nodes and the coarsest 19 nodes. This method allows us to keep the mesh size ratio close to 2, and a comparable local mesh aspect ratio. The intergrid transfer operators [9] are linear interpolations, concerning the variables and the corrections, and linear distributions, concerning the residuals. The MG algorithm will be the W-cycle, because it is the natural extension of the ideal-2-grid scheme. Furthermore, there exist several ways to obtain 2nd-order accurate solutions:

- Mavriplis [10] uses an FMG algorithm, where 1st-order accurate solutions are computed on the coarse levels, and 2nd-order accurate on the finest. Some experiments with our upwind schemes showed us that the convergence speed is hardly independent of the mesh size.

- Hemker-Koren [11] propose to get a 1st-order solution with an FMG strategy and then to compute a certain number of DeCV-cycles: They use the Defect Correction (DeC) algorithm

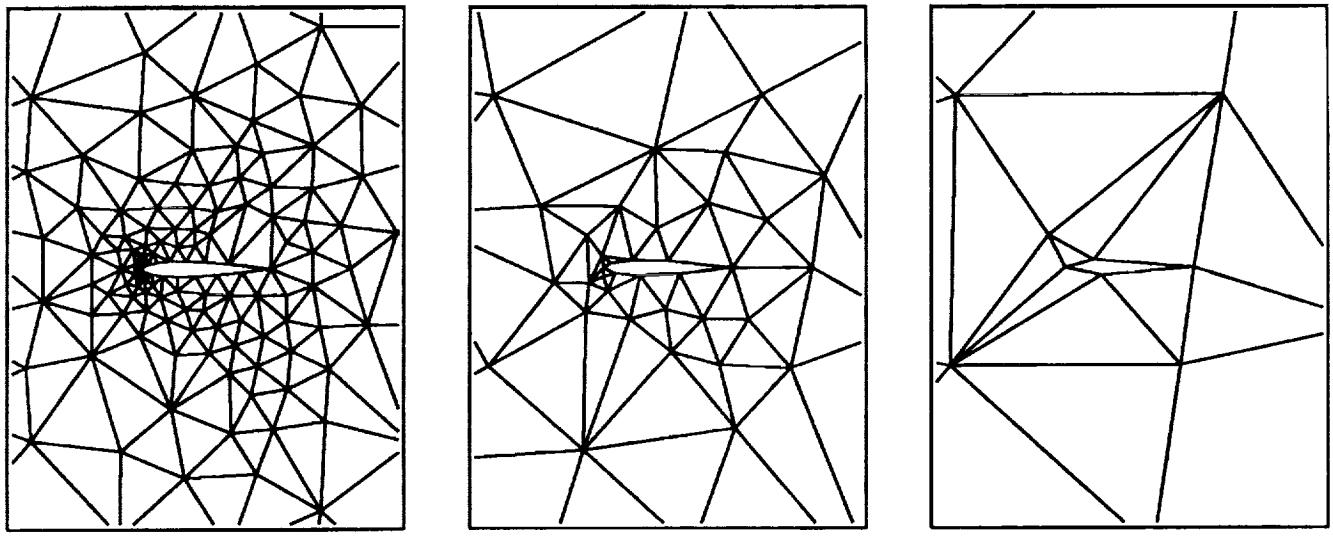

a. 223 nodes b. 67 nodes c. Coarsest 19 nodes

Figure 2: NACA0012 coarse meshes.

[12], in order to solve the 2nd-order accurate following problem: $\mathcal{F}_2(W) = S$. It is written:

$$\begin{aligned} &\mathcal{F}_1(W^1) = S\ , \\ &\mathcal{F}_1(W^{N+1}) = \mathcal{F}_1(W^N) - \mathcal{F}_2(W^N) + S\ ,\quad N = 1\ ,\ 2\ ,\ \ldots \end{aligned} \tag{10}$$

Actually, we define the DeCV-cycling method where the 1st-order problem in (10) is approximately solved with one V-cycle. However, we do not know how many DeCV-cycles are to be performed and we lose the $O(N)$ complexity.

We propose here two different methods in order to obtain 2nd-order accurate solutions with an $O(N)$ complexity algorithm [1].

- FMDeCV is an FMG strategy where we use DeCV-cycles in each phase, with two Jacobi sweeps per level (FMDeCV-2RK1).
- FMG2 is an FMG strategy where we use on each level of the different phases the good damping properties of the multistage schemes (see [13]) for smoothing directly the second order accurate problem.

A result of convergence of the DeCV method is given in [14] and assures that DeCV-cycling has a convergence speed independent of the mesh size:

$$\|DeCVu_h^\alpha - \bar{u}_h^2\| < S_2\ \|u_h^\alpha - \bar{u}_h^2\|\ ,\ S_2 = S_1 + S_1 S_{DeC} + S_{DeC} < 1 \tag{11}$$

where $DeCVu_h^\alpha$ is the $\alpha-$th iterate of the DeCV-cycling and $\bar{u}_h^2$ is the solution of the 2nd-order accurate problem.

Remark: Desideri-Hemker in [12] show that the convergence speed S_{DeC} of the DeC process is at least equal to 1/2. From (11), we should use MG 1st-order accurate algorithms whose convergence

speed S_1 (independent of the mesh size) is less than 1/3. Actually, the experiments showed us that $S_1 > 1/3$ does not induce difficulty.

SECOND ORDER ACCURATE RESULTS

Euler Flows around a NACA0012 profile

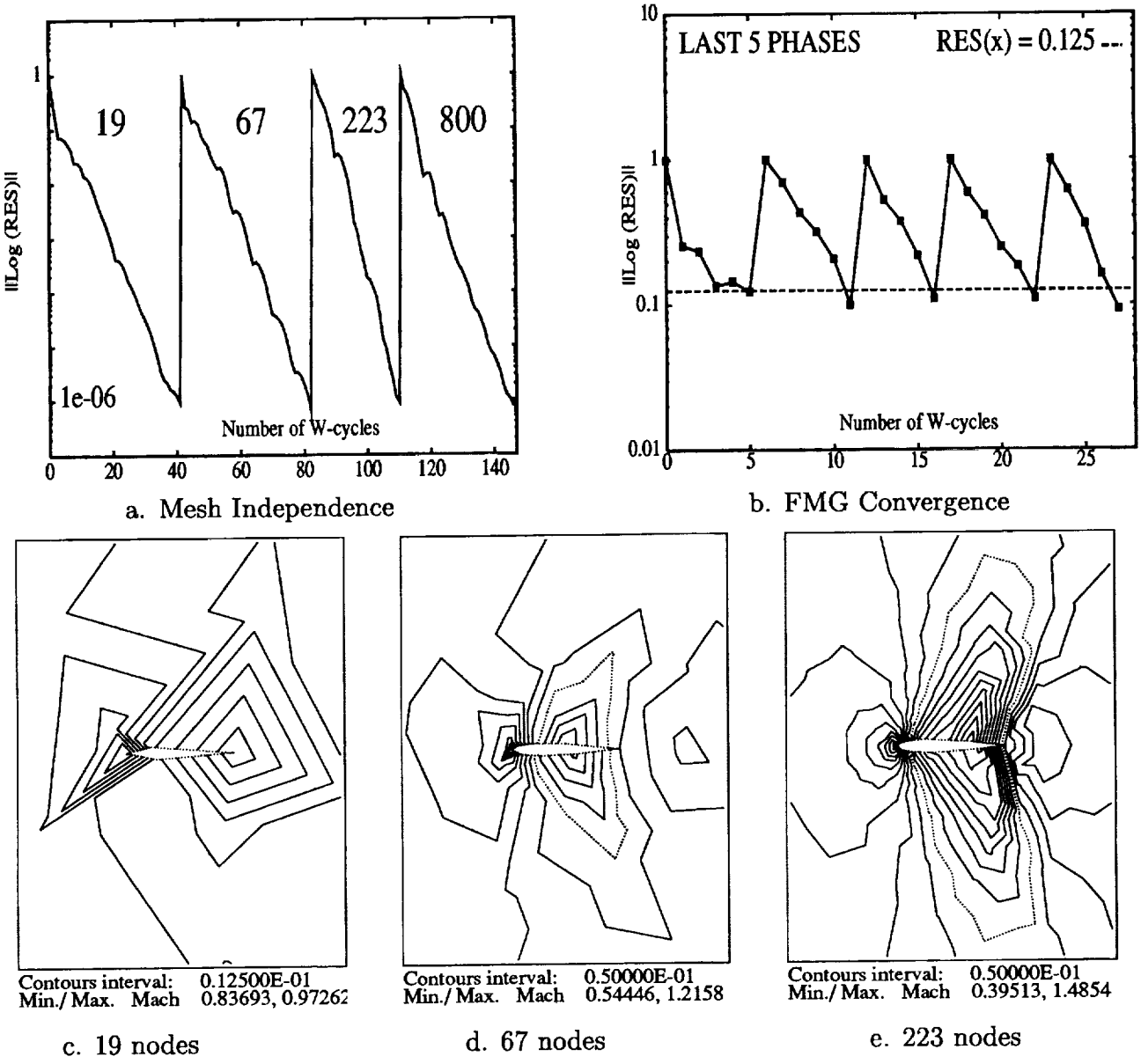

a. Mesh Independence

b. FMG Convergence

c. 19 nodes

d. 67 nodes

e. 223 nodes

Figure 3: Euler FMG2 phases, isomach contours, $M_\infty = 0.9$, $\alpha = 0^o$.

The test-case depicted in Fig.3 to Fig.5 is defined by a farfield Mach number equal to 0.9, and a zero angle of attack. The smoother is the (4 stage) RKJ one, whose coefficients ($\alpha_1 = 0.14, \alpha_2 =$

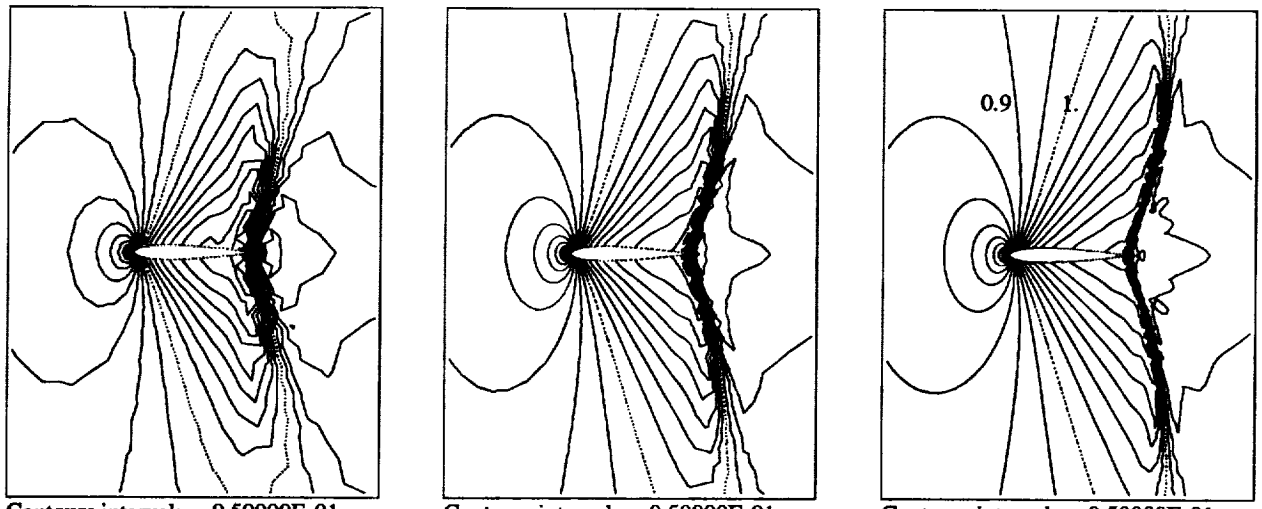

a. 800 nodes b. 3114 nodes c. 12284 nodes

Figure 4: Euler FMG2 phases, isomach contours, $M_\infty = 0.9$, $\alpha = 0^o$.

$0.2939, \alpha_3 = 0.5252, \alpha_4 = 1$) are due to van Leer [15], and defines the FMG2 strategy. In Fig.3.a, we present the convergence histories of the logarithm of the residual versus the number of cycles in each phase. The convergence is estimated as obtained when the residual decrease reaches 10^{-6}. The first history is a 1-grid convergence on the coarsest mesh (19 nodes), the last (4-grid scheme) on the 800 node mesh. At the end of the convergence of each phase we produce an initialization of the next phase by interpolating the solution on the next finer mesh. We may notice that the different convergence histories tend to be straight lines with the same value of slope: this allows us to say that the convergence speed is independent of the mesh-size and that we may use an FMG strategy. In Fig.3.b the residual convergence histories of the last 5 phases are depicted (the first one is a 1-grid convergence history with a residual decrease equal to 10^{-6}). In order to neglect oscillatory non-linear phenomena we choose to impose a residual decrease equal to 1/8 (and not a defined number of cycles): the FMG convergence histories follow exactly the peaks of the (corresponding) phases on Fig.3.a, and, the solutions are not either changed. A solution on the finest grid (Fig.1.c) is reached after only 5 cycles (77 WU, 673 s on Convex C210 with non vectorized software). In Fig.3 and Fig.4 we show the different solutions obtained at the end of each phase: they are non-symmetrical solutions (Fig.3), due to the fact that the coarse meshes are non-symmetrical. However, this phenomenon vanishes when the different meshes become symmetrical (Fig.4). Another important remark is that the solution between the finest mesh and the next coarser one does not vary much: we may say that we get a nearly converged solution on the 3114 node mesh. In order to verify the previous assumption, we compare the FMG solution of Fig.5 with the solution obtained after a 10^{-6} residual decrease: the Mach number extrema are approximately the same although the isomach lines are a little bit more oscillatory for the FMG solution.

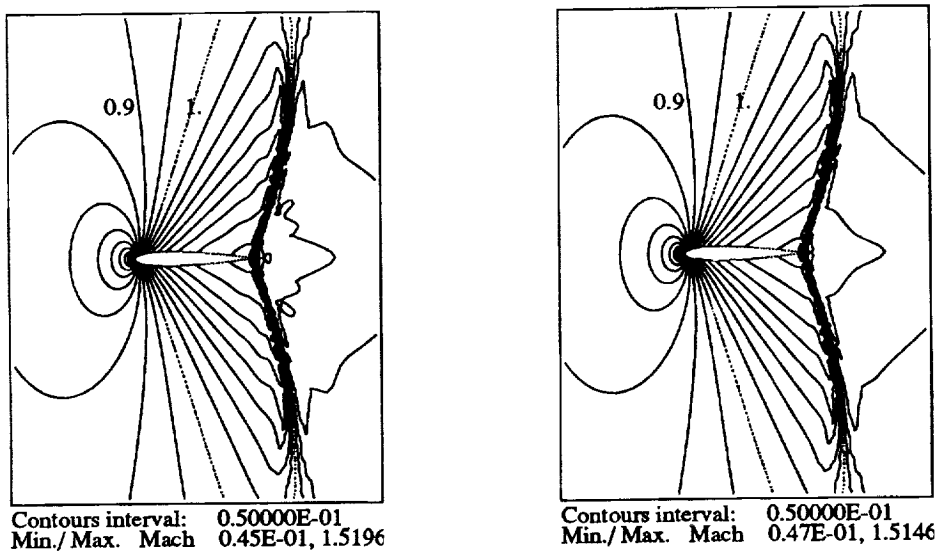

a. FMG2 b. Converged (RES = 10^{-6})

Figure 5: Euler FMG2 solutions, isomach contours, $M_\infty = 0.9$, $\alpha = 0^o$.

Navier-Stokes Flows around a NACA0012 profile

The first test-case is defined by a farfield Mach number equal to 0.8, an angle of attack equal to 10 degrees and a Reynolds number equal to 73. We use here an FMDeCV-2RK1 strategy (justified by the mesh independent convergence of Fig.6.a). The solution (Fig.6.c) is obtained on the finest mesh after 4 cycles that represent 42 WU computation and a total CPU time equal to 537 s. In Fig.6.d we illustrate the behavior of the pressure lift, CL (drag,CD) coefficient with a solid (dash) line, versus the number of finest-grid iterations, up to a residual decrease on the finest grid of 10^{-12}. The points (cross) represent these coefficients during the FMG process, thus up to a 0.125 residual decrease. We can notice that the value of each of them is almost obtained at the end of the FMG phase (the error is equal to 64.10^{-5} for the CL coefficient and to 16.10^{-5} for the CD coefficient).

The second test-case, presented in Fig.7, is defined by a farfield Mach number equal to 2, an angle of attack equal to 10 degrees, and a Reynolds number equal to 106. This time we use an FMG2 strategy (more robust than FMDeCV-2RK1 that needs TVD limitation and implies that the residual stalls from the value of 10^{-3}); this produces a solution after 7 cycles (Fig.7.c, 109 WU, 1862 s), and we can make the same remarks as in the previous test-cases. The next coarser mesh results in CL and CD values within 1% of their final values which are obtained after 7 cycles on the finest mesh with a related error respectively of 2.10^{-6} and 2.10^{-5} (Fig.7.d),

The last test-case shows us one limitation of this method. It is defined by a farfield Mach number equal to 0.8, an angle of attack equal to 10 degrees and a Reynolds number equal to 500. Here again, we use an FMDeCV-2RK1 strategy (Fig.8). We may note, once again, that the FMG convergence histories (Fig.8.b) look like the corresponding peaks on Fig.8.a, thus we think that the solution does not vary between a 10^{-1} residual decrease and a 10^{-6} one. However, on Fig.9.a we note that the isomach lines are deformed up until the last solution (Fig.9.c) which presents two bumps. Actually,

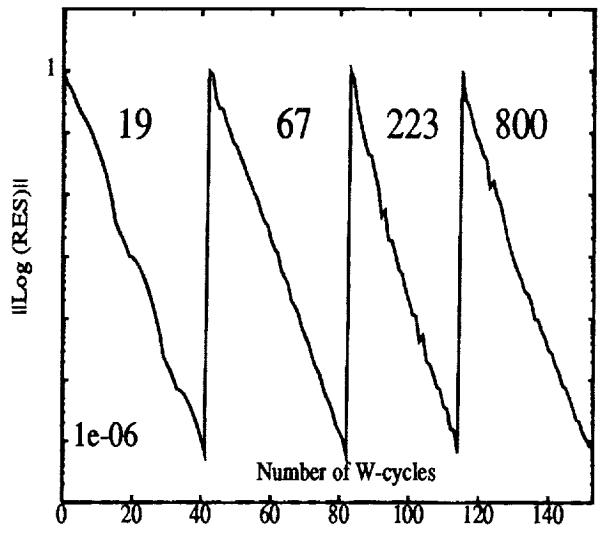

a. Mesh Independence

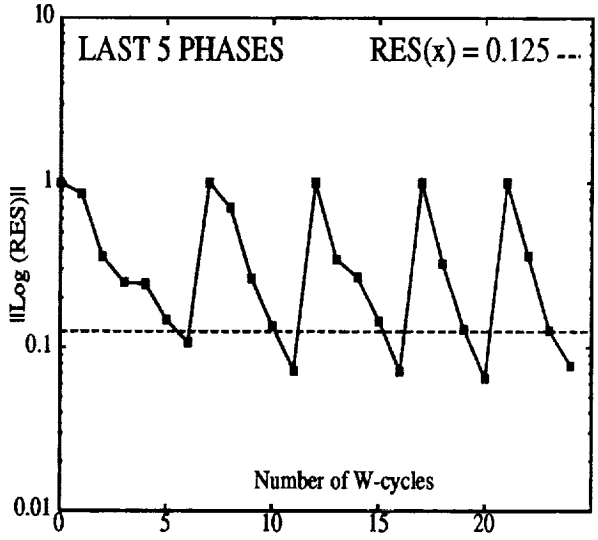

b. FMG Convergence

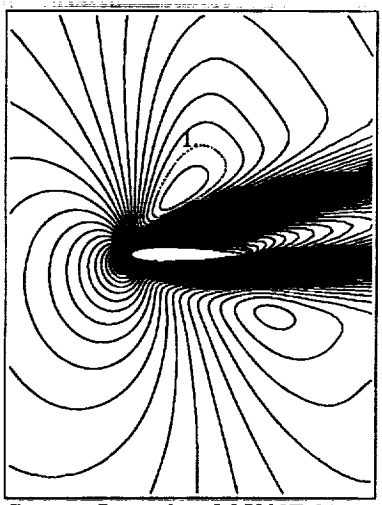

c. Isomach contours

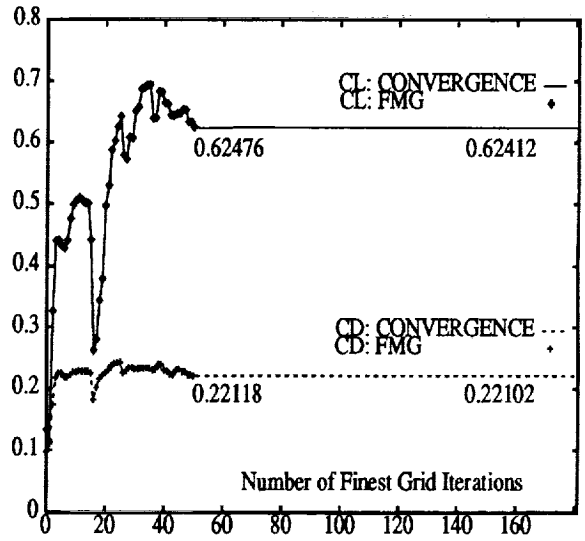

d. CL and CD behaviors

Figure 6: Navier-Stokes FMDeCV-2RK1 solution, $M_\infty = 0.8$, $\alpha = 10^o$, $Re = 73$.

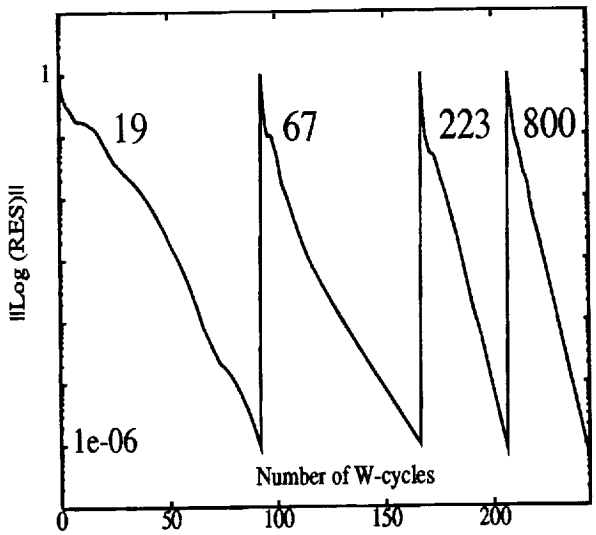

a. Mesh Independence

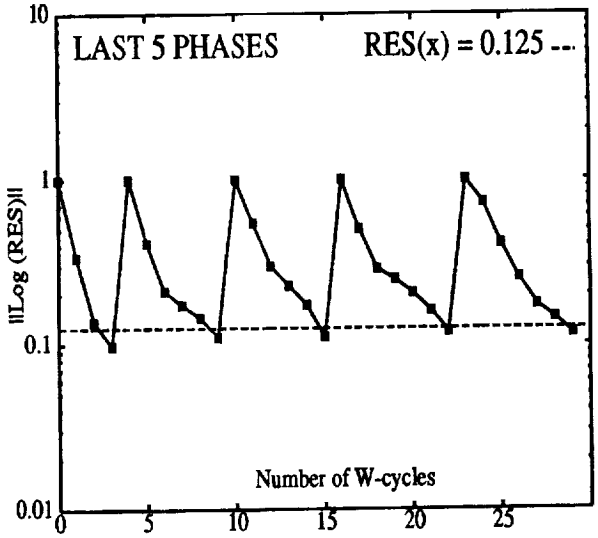

b. FMG Convergence

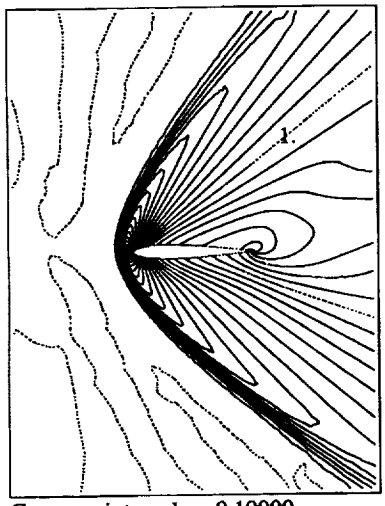

c. Density contours

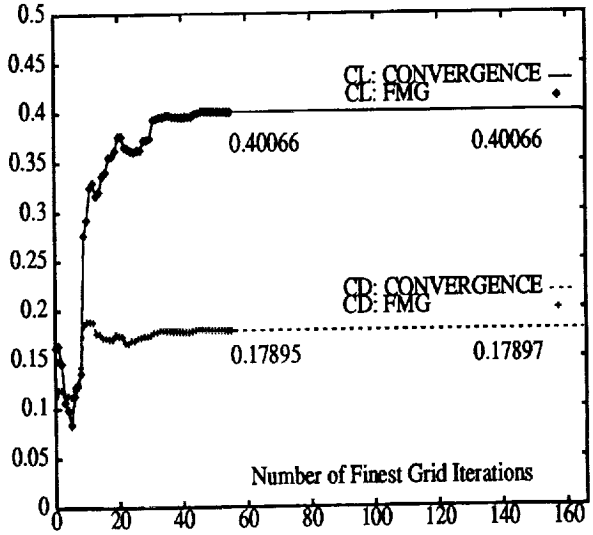

d. CL and CD behaviors

Figure 7: Navier-Stokes FMG2 solution, $M_\infty = 2$, $\alpha = 10^o$, $Re = 106$.

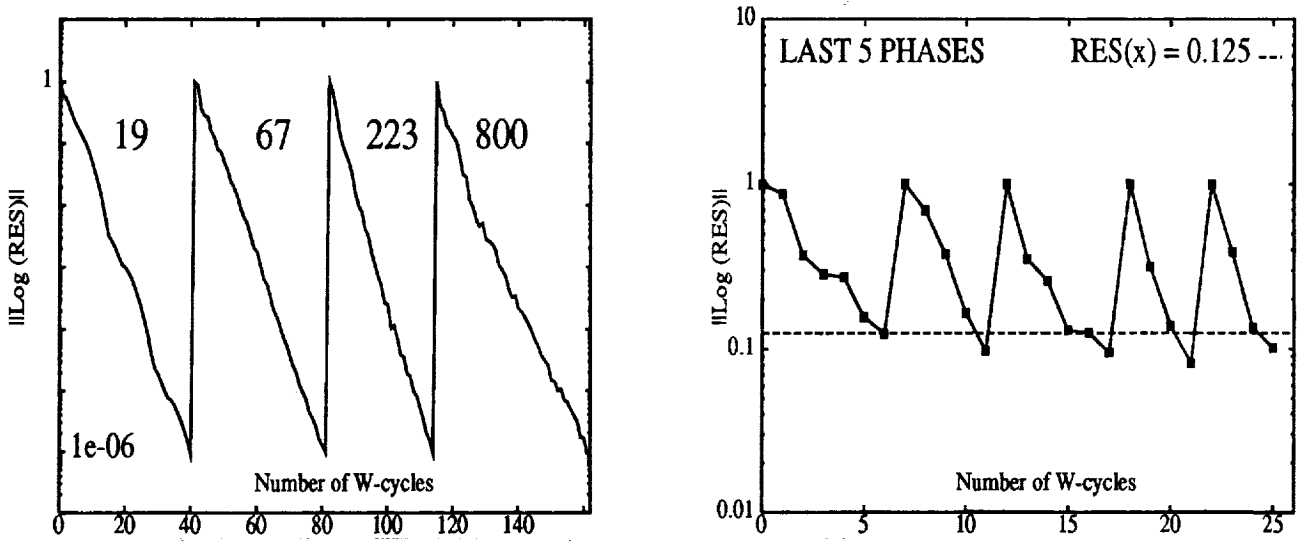

a. Mesh Independence

b. FMG Convergence

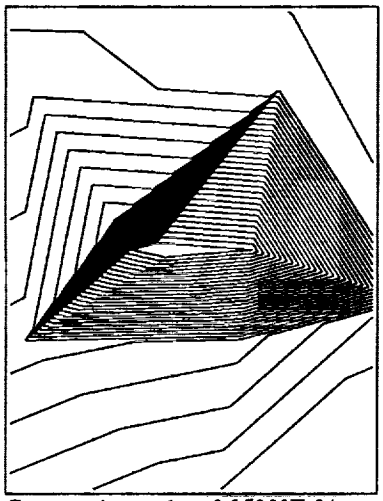

Contours interval: 0.25000E-01
Min./ Max. Mach 0. , 0.79407

c. 19 nodes

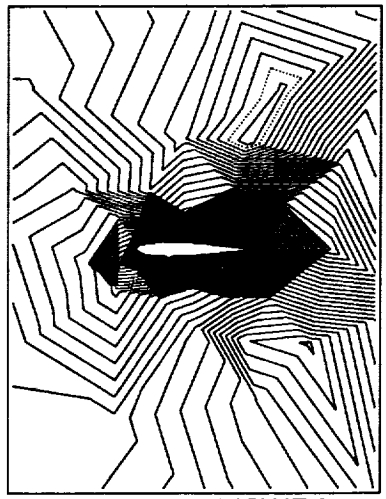

Contours interval: 0.25000E-01
Min./ Max. Mach 0. , 1.0496

d. 67 nodes

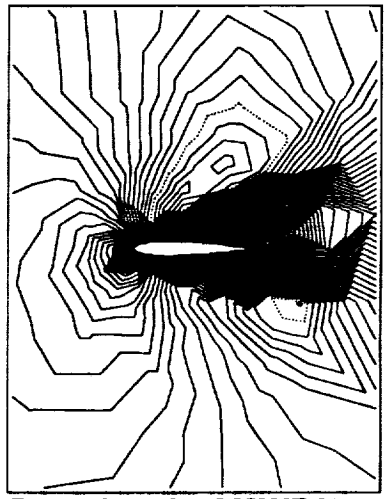

Contours interval: 0.25000E-01
Min./ Max. Mach 0. , 1.0901

e. 223 nodes

Figure 8: Navier-Stokes FMDeCV-2RK1 phases, isomach contours, $M_\infty = 0.8$, $\alpha = 10°$, $Re = 500$.

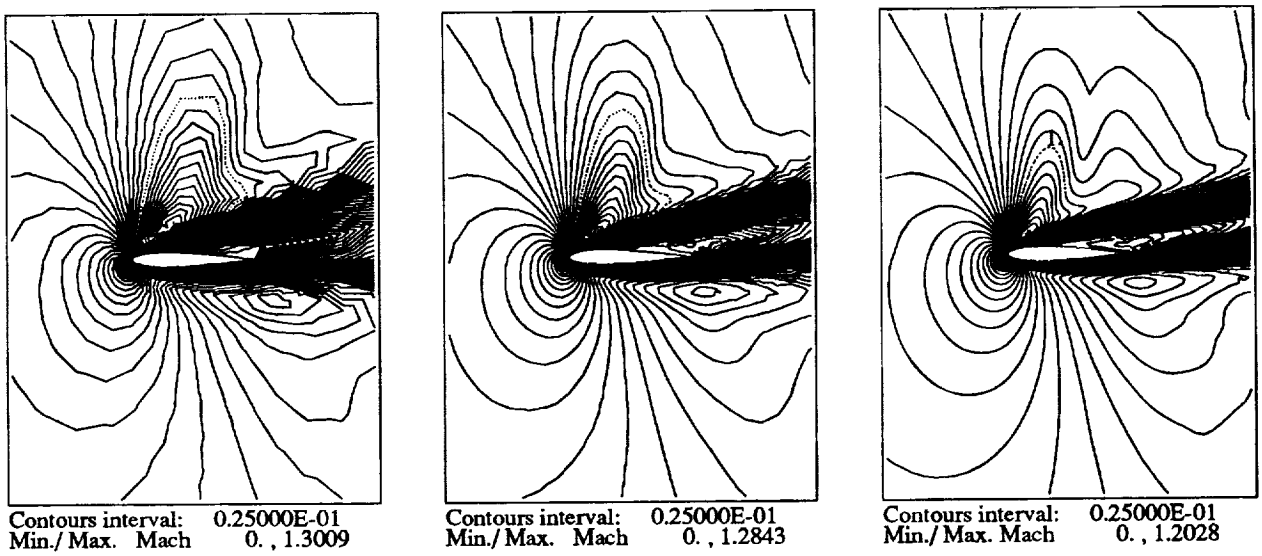

a. 800 nodes b. 3114 nodes c. 12284 nodes

Figure 9: Navier-Stokes FMDeCV-2RK1 phases, isomach contours, $M_\infty = 0.8$, $\alpha = 10^o$, $Re = 500$.

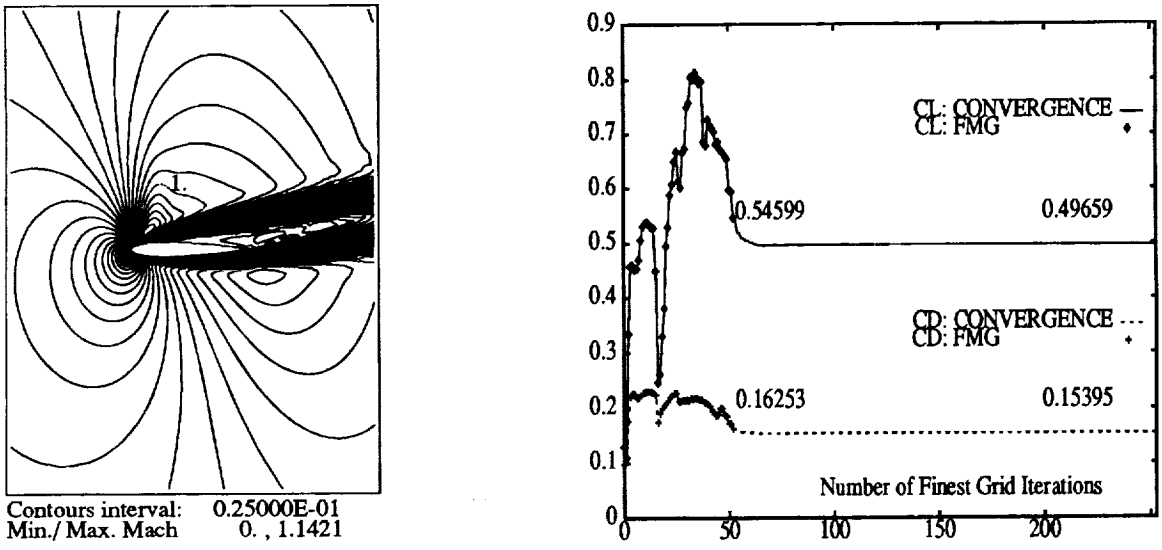

a. Isomach contours b. CL and CD behaviors

Figure 10: Navier-Stokes FMDeCV-2RK1 solution, $M_\infty = 0.8$, $\alpha = 10^o$, $Re = 500$.

since the solution differs a lot between the one obtained on the finest mesh and the other on the next coarser mesh (Fig.9.c and .b), we may say that we did not obtain a grid-converged solution. Furthermore, these two humps may be justified because the meshes that we use (especially the coarse ones) are not adapted for such a viscous flow and may not capture the boundary layer. Our assumption is confirmed by the CL and CD behaviors (Fig.10.b), where we note an error for the CL coefficient equal to 5.10^{-2} and for the CD coefficient equal to 8.10^{-3}. Moreover, we get a solution (Fig.10.a) after 105 cycles (1107 WU, 14112 s), for a residual decrease of 10^{-12} and which tends to confirm that the FMG solution is not a steady solution.

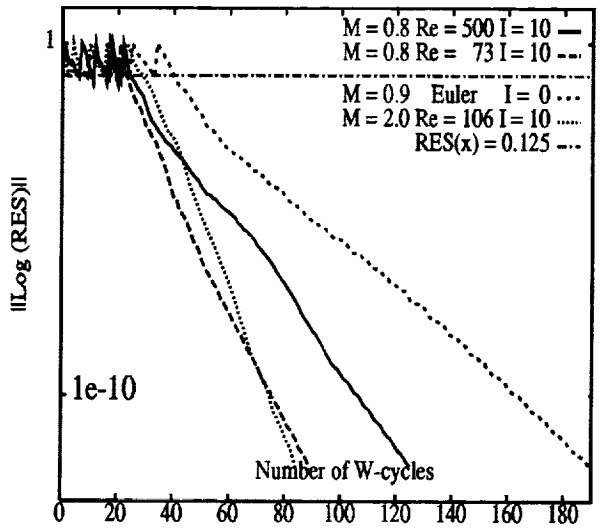

Figure 11: Convergences

CONCLUSION

We want to point out that the use of FMG2 or FMDeCV strategy allowed us to get 2nd-order accurate solutions in most of cases with a limited number of operations ($O(N)$ complexity). FMDeCV-2RK1 is more adapted to smooth problems and costs half as much as FMG2. Furthermore, we had to use an entropy correction technique [16] to get the above results, and occasionally a 10^{-12} residual decrease required to increase the value of this correction to prevent the residual from stalling or to improve robustness on the finest grid (this increased slightly the number of cycles in each phase without changing the solution greatly). As depicted in Fig.11, these types of computations do not induce any stall during the convergence. The main two difficulties, non-embedded meshes and the requirement of 2nd-order accuracy, were remedied, respectively, by using a coarsening algorithm based on a Voronoï technique, and basic iteration techniques that were sufficient smoothers. The difficulty encountered in using an FMG strategy, with our meshes, increased as the Reynolds number was raised. Actually, it is obvious that our meshes are not adapted to these computations and that boundary layer problems will need the production of stretched meshes and different specialized smoothers, as suggested in [14].

ACKNOWLEDGEMENTS

The meshes were kindly given by Hervé Guillard. A part of the MG codes was initiated by Marie-Pierre Leclercq and Bruno Stoufflet. We thank Piet Hemker, Barry Koren, Marie-Hélène Lallemand and Dimitri Mavriplis for the many helpful discussions we had with them.

References

[1] W. HACKBUSCH, *"Multi-Grid Methods and Applications"*, Springer Series in Comp. Math., Springer Verlag, Vol. 4, (1985).

[2] E. MORANO, M.H. LALLEMAND, M.P. LECLERCQ, H. STEVE, B. STOUFFLET A. DERVIEUX, *"Local iterative upwind methods for steady compressible flows"*, GMD-Studien Nr. 189, Multigrid Methods: Special Topics and Applications II, 3rd Europ. Conf. on Multigrid Methods, Bonn 1990 (1991).

[3] S. ZHANG, *"Multi-level iterative techniques"*, PhD Thesis, The Pensylvania State University (1988).

[4] A. BRANDT, *"Guide to multigrid development"*, Multigrid Methods, Proc. of the Köln-Porz Conf. on Multigrid Methods, (W. Hackbusch and U. Trottenberg, Eds.), Lect. Notes in Math. 960, Springer, Berlin, p. 220-312 (1982).

[5] S. LANTERI, *"Simulation d'écoulements aérodynamiques instationnaires sur une architecture massivement parallèle"*, PhD Thesis, Université de Nice Sophia-Antipolis (1991).

[6] B. van LEER, *"Flux vector splitting for the Euler equations"*, Lect. Notes in Phys., Vol. 170, p. 405-512 (1982).

[7] E. DICK, K. RIEMSLAGH, *"Multi-stage Jacobi relaxation as smoother in a multigrid method for steady Euler equations"*, Proc. of ICFD Conf. on Num. Methods for Fluid Dynamics, Reading, England (1992).

[8] E. MORANO, H. GUILLARD, A. DERVIEUX, M.P. LECLERCQ, B. STOUFFLET, *"Faster relaxations for non-structured MG with Voronoï coarsening"*, Comput. Fluid Dynamics '92, Proc. of the first Europ. Comput. Fluid Dynamics Conf., Brussels, Belgium, (Ch. Hirsch, J. Périaux, W. Kordulla Eds.), Vol. I, p. 69-74, ECCOMAS, ELSEVIER (1992).

[9] M.-P. LECLERCQ, B. STOUFFLET, *"Characteristic Multigrid Method Application to solve the Euler equations with unstructured and unnested grids"*, Inter. Conf. on Hyperbolic Problems, Uppsala (1989).

[10] D. MAVRIPLIS, A. JAMESON, *"Multigrid solution of the Navier-Stokes equations on triangular meshes"*, ICASE Report No. 89-11 (1989).

[11] B. KOREN, P.W. HEMKER, *"Damped, direction-dependent multigrid for hypersonic flow computations"*, Appl. Num. Math., North-Holland, Vol. 7, p. 309-328 (1991).

[12] J.A. DESIDERI, P. HEMKER, *"Analysis of the convergence of iterative implicit and Defect–Correction algorithms for hyperbolic problems"*, INRIA Research Report 1200 (1990).

[13] M.H. LALLEMAND, *"Schémas décentrés multigrilles pour la résolution des équations d'Euler en éléments finis"*, PhD Thesis, Université de Marseille (1988).

[14] E. MORANO, *"Résolution des équations d'Euler par une méthode multigrille stationnaire"*, PhD Thesis, Université de Nice Sophia-Antipolis (1992).

[15] B. van LEER, C.H. TAI, and K.G. POWELL, *"Design of optimally-smoothing multi-stage schemes for the Euler equations"*, AIAA in 9th Comput. Fluid Dynamics Conf., 89-1933-CP (1989).

[16] A. HARTEN, *"High Resolution Schemes for Hyperbolic Conservation Laws"*, J. Comput. Phys., Vol. 49, p. 357-393 (1983).